


**Please cite the Published Version**

Du, Jianhe, Luo, Xin, Li, Xingwang, Zhu, Mingfu, Rabie, Khaled M  and Kara, Ferdi (2023) Semi-blind joint channel estimation and symbol detection for RIS-empowered multiuser mmWave Systems. IEEE Communications Letters, 27 (1). pp. 362-366. ISSN 1089-7798

**DOI:** <https://doi.org/10.1109/LCOMM.2022.3212083>

**Publisher:** Institute of Electrical and Electronics Engineers

**Version:** Accepted Version

**Downloaded from:** <https://e-space.mmu.ac.uk/632946/>

**Usage rights:**  In Copyright

**Additional Information:** © 2022 IEEE. Personal use of this material is permitted. Permission from IEEE must be obtained for all other uses, in any current or future media, including reprinting/republishing this material for advertising or promotional purposes, creating new collective works, for resale or redistribution to servers or lists, or reuse of any copyrighted component of this work in other works.

**Enquiries:**

If you have questions about this document, contact [rsl@mmu.ac.uk](mailto:rsl@mmu.ac.uk). Please include the URL of the record in e-space. If you believe that your, or a third party's rights have been compromised through this document please see our Take Down policy (available from <https://www.mmu.ac.uk/library/using-the-library/policies-and-guidelines>)

# Semi-Blind Joint Channel Estimation and Symbol Detection for RIS-Empowered Multiuser mmWave Systems

Jianhe Du, Xin Luo, Xingwang Li, Mingfu Zhu, Khaled M. Rabie, and Ferdi Kara,

**Abstract**—In this letter, we propose a semi-blind joint channel estimation and symbol detection scheme for reconfigurable intelligent surface (RIS)-empowered multiuser millimeter wave (mmWave) systems. Combined with the coding scheme at user equipments (UEs) and RIS reflection coefficient design, we prove that the received signals at the base station (BS) follow a PARATUCK2 tensor model, and then a two-stage fitting algorithm is derived by exploiting the low-rank structure of mmWave channel. Without a dedicated training stage, the proposed scheme can jointly detect information symbols of all UEs and estimate the channels of the UEs-RIS and RIS-BS links. In comparison to the existing methods, the proposed system can increase spectrum efficiency and obtain better channel estimation and symbol detection performance. Numerical results are presented to verify the effectiveness of the proposed scheme.

**Index Terms**—Joint estimation and detection, RIS, mmWave, PARATUCK2 tensor, low-rank.

## I. INTRODUCTION

MILLIMETER wave (mmWave) communication achieves unprecedented gigabits-per-second data rates with abundant spectrum resources, which makes it a promising technology to keep up with rapid the growth of transmission speed demand in wireless communications [1]. However, the communication distance is severely restricted owing to high path loss in mmWave bands and severe blockage problems. To address this, promising solutions such as reconfigurable intelligent surfaces (RISs) have been developed.

Integrating the RIS into wireless networks brings new challenges from a communication standpoint, e.g., channel estimation, RIS beamforming design and deployment. In particular, accurately estimating channel state information (CSI) deserves further investigation. A three-phase pilot-based channel estimation framework is proposed in [2] to estimate the cascaded UE-RIS-BS links. However, in order to optimize the RIS-empowered system, the information of both UE-RIS and RIS-BS links is required. In [3], two schemes are proposed to realize channel estimation, where both channel

links can be estimated separately. However, this method is only applicable to time-division duplexing (TDD) systems. Recently, tensor decomposition has been considered to be an effective method for channel estimation in RIS-empowered systems [4], [5]. The work in [4] presents two tensor-based channel estimation techniques composed of the alternating least squares (ALS) algorithm and the vector approximate message passing (VAMP) algorithm. In [5], a receiver design is addressed by presenting two channel estimation methods including the Khatri-Rao factorization (KRF) algorithm and the iterative bilinear ALS (BALS) algorithm. The tensor-based methods [4], [5] are applicable to both the TDD and frequency division duplexing (FDD) systems.

However, the aforementioned schemes [2]–[5] incur a large number of pilot overhead stemming from the acquisition of CSI, which leads to a decline in spectrum efficiency. To reduce the pilot overhead, joint channel estimation and signal recovery is realized in [6] by bidirectional two-layer algorithms. Different from the matrix-based method in [6], the work in [7] develops a tensor-based semi-blind KAKF algorithm, which is composed of the KRF and the Kronecker factorization (KF) methods for joint channel and signal estimation. Although the KAKF algorithm without any iterative procedures has a low computational complexity, it cannot estimate all parameters simultaneously and the error propagation problem will occur since the estimation performance of the second stage depends largely on that of the first stage. Thus, it is necessary to further improve the accuracy of joint channel estimation and symbol estimation for RIS-empowered systems, especially in higher-frequency bands.

In this letter, we first design a PARATUCK2 tensor model for RIS-empowered multiuser mmWave systems. Then a two-stage fitting algorithm is proposed to provide the base station (BS) with full knowledge of channel matrices and information symbols. The main contributions of this letter are summarized below:

- By exploiting the algebraic structure of the constructed PARATUCK2 tensor model, the proposed scheme makes full use of the tensor decomposition technology to acquire full knowledge of CSI involved in the communication and information symbols of all UEs without a dedicated training stage.
- By utilizing the hybrid Kronecker/Khatri-Rao factorization and the low-rank structure of the mmWave channel, the proposed scheme provides higher spectrum efficiency in contrast to the pilot-assisted methods [2]–[5], and

Jianhe Du and Xin Luo are with the State Key Laboratory of Media Convergence and Communication, Communication University of China, Beijing 100024, China (email: dujianhe1@gmail.com and luoxin\_cuc@cuc.edu.cn).

Xingwang Li and Mingfu Zhu are with the School of Physics and Electronic Information Engineering, Henan Polytechnic University, Jiaozuo 454000, China (email: lixingwang@hpu.edu.cn and zhumingfu@zzu.edu.cn).

Khaled M. Rabie is with the Department of Engineering, Manchester Metropolitan University, M1 5GD Manchester, U.K. (e-mail: K.Rabie@mmu.ac.uk).

Ferdi Kara is with the Department of Computer Engineering Incivez, Zonguldak Bulent Ecevit University, Zonguldak 67100, Turkey (e-mail: f.kara@beun.edu.tr).

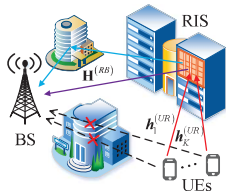


Fig. 1. The RIS-empowered multiuser mmWave system.

has higher fitting accuracy compared to the semi-blind methods [6], [7].

- We analyze the uniqueness issue and the identifiability conditions of the constructed PARATUCK2 tensor model. The proposed scheme requires a more relaxed identifiability condition than that in [7]. In addition, monte Carlo simulation results show that the proposed scheme improves the estimation and detection accuracy compared to existing methods.

*Notations:* Lower-case letters ( $a, b, \dots$ ) denote scalars, boldface lower-case letters ( $\mathbf{a}, \mathbf{b}, \dots$ ) denote matrices and calligraphic letters ( $\mathcal{A}, \mathcal{B}, \dots$ ) denote tensors. The transpose, conjugate, Hermitian transpose and pseudo-inverse of  $\mathbf{A}$  are represented by  $\mathbf{A}^T$ ,  $\mathbf{A}^*$ ,  $\mathbf{A}^H$ , and  $\mathbf{A}^\dagger$ , respectively.  $a_{m,n}$  stands for the  $(m, n)$ -th entry of  $\mathbf{A} \in \mathbb{C}^{M \times N}$ . Both  $\mathbf{a}_n$  and  $\mathbf{A}(:, n)$  represent the  $n$ -th column of  $\mathbf{A}$ .  $\text{vec}(\cdot)$  denotes a vector out of the diagonal of its matrix argument.  $\otimes$  and  $\odot$  represent the Kronecker product and Khatri-Rao product, respectively. The following properties are used throughout this letter:

$$\text{vec}(\mathbf{ABC}) = (\mathbf{C}^T \otimes \mathbf{A}) \text{vec}(\mathbf{B}), \quad (1)$$

$$\text{vec}(\mathbf{BD}_m(\mathbf{A})\mathbf{C}) = (\mathbf{C}^T \odot \mathbf{B}) \mathbf{A}_m^T, \quad (2)$$

where the sizes of the matrices  $\mathbf{A}$ ,  $\mathbf{B}$  and  $\mathbf{C}$  are suitable for mathematical operations.

## II. SYSTEM MODEL

### A. Channel Model

As shown in Fig. 1, we consider a RIS-empowered multiuser mmWave uplink system with  $K$  single-antenna user equipments (UEs), a RIS consisting of  $N$  elements and a BS with  $M$  antennas. It is assumed that the line-of-sight (LoS) paths between the UEs and BS are unavailable [1]. Both the RIS and the BS employ uniform planer array (UPA). It is assumed that there are  $L_{UR,k}$  and  $L_{RB}$  resolvable paths from the  $k$ -th UE to the RIS and from the RIS to the BS, respectively. For mmWave systems, the values of  $L_{UR,k}$  and  $L_{RB}$  are both small since the signals usually suffer serious path loss in the transmission process, and reflect less to the surrounding environment [8]. Let  $\mathbf{h}_k^{(UR)} \in \mathbb{C}^{N \times 1}$  be the channel between the  $k$ -th UE and the RIS,  $k = 1, \dots, K$ . We employ the widely utilized Saleh-Valenzuela channel model to represent  $\mathbf{h}_k^{(UR)} \in \mathbb{C}^{N \times 1}$  as [9]

$$\mathbf{h}_k^{(UR)} = \sqrt{\frac{N}{L_{UR,k}}} \sum_{l_{UR,k}=1}^{L_{UR,k}} \alpha_{l_{UR,k}}^k \mathbf{a}_R(\theta_{l_{UR,k}}^{R_{UR,k}}, \varphi_{l_{UR,k}}^{R_{UR,k}}), \quad (3)$$

where  $\alpha_{l_{UR,k}}^k$  and  $\theta_{l_{UR,k}}^{R_{UR,k}}(\varphi_{l_{UR,k}}^{R_{UR,k}})$  are the complex path gain and the azimuth (elevation) angle at the RIS associated with

the  $l_{UR,k}$ -th path, respectively. Similarly, the channel  $\mathbf{H}^{(RB)} \in \mathbb{C}^{M \times N}$  between the RIS and the BS can be modeled as

$$\mathbf{H}^{(RB)} = \sqrt{\frac{MN}{L_{RB}}} \sum_{l_{RB}=1}^{L_{RB}} \beta_{l_{RB}} \mathbf{a}_B(\theta_{l_{RB}}^{B_{RB}}, \varphi_{l_{RB}}^{B_{RB}}) \mathbf{a}_R^T(\theta_{l_{RB}}^{R_{RB}}, \varphi_{l_{RB}}^{R_{RB}}), \quad (4)$$

where  $\beta_{l_{RB}}$ ,  $\theta_{l_{RB}}^{B_{RB}}(\varphi_{l_{RB}}^{B_{RB}})$  and  $\theta_{l_{RB}}^{R_{RB}}(\varphi_{l_{RB}}^{R_{RB}})$  are the complex path gain, the azimuth (elevation) angle at the BS and the azimuth (elevation) angle at the RIS associated with the  $l_{RB}$ -th path, respectively. Ignoring the superscripts and subscripts,  $\mathbf{a}_R(\theta, \varphi)$  and  $\mathbf{a}_B(\theta, \varphi)$  are the normalized array steering vectors. Without loss of generality, for a typical  $F_1 \times F_2$  UPA,  $\mathbf{a}(\theta, \varphi)$  is obtained by

$$\mathbf{a}(\theta, \varphi) = \frac{1}{\sqrt{F}} \left[ 1, e^{-j\omega}, \dots, e^{-j(F_1-1)\omega} \right]^T \otimes \left[ 1, e^{-j\psi}, \dots, e^{-j(F_2-1)\psi} \right]^T, \quad (5)$$

where  $F = F_1 \times F_2$ ,  $\omega = 2\pi d \sin \theta \cos \varphi / \lambda$ ,  $\psi = 2\pi d \sin \varphi / \lambda$ ,  $\lambda$  is the carrier wavelength and  $d$  is the antenna spacing which is normally set to  $\lambda/2$ .

### B. PARATUCK2 Signal Model

Denote  $\mathbf{s}_k \in \mathbb{C}^{T \times 1}$  as the transmitted symbol vector of the  $k$ -th UE, where  $T$  is the length of the information symbol. Let  $\mathbf{e}_k \in \mathbb{C}^{P \times 1}$  be the coding vector associated with the  $k$ -th UE, where  $P$  is the number of the time blocks of the overall signal transmission period. The block-fading channel is adopted, which implies that the channel coefficients remain unchanged over the coherence time interval. It can be concluded that the coherence time is  $T_C = TP$ . Denote  $\phi_p = [\phi_{1,p}, \dots, \phi_{N,p}]^T \in \mathbb{C}^{N \times 1}$  as the phase shift vector that simulates the RIS phase shifts and activation pattern, and let  $D_p(\Phi) = \text{diag}(\phi_p)$  be a diagonal matrix with the  $p$ -th row of the RIS phase shift matrix  $\Phi \in \mathbb{C}^{P \times N}$  forming its diagonal,  $p = 1, \dots, P$ . At the BS, the received signal forms the  $p$ -th frontal slice  $\mathbf{Y}_p \in \mathbb{C}^{M \times T}$  of a third-order tensor  $\mathcal{Y} \in \mathbb{C}^{M \times P \times T}$  as

$$\begin{aligned} \mathbf{Y}_p &= \mathbf{H}^{(RB)} D_p(\Phi) \sum_{k=1}^K \left( \mathbf{h}_k^{(UR)} D_p(\mathbf{e}_k) \mathbf{s}_k^T \right) + \mathbf{V}_p \\ &= \mathbf{H}^{(RB)} D_p(\Phi) \mathbf{H}^{(UR)} D_p(\mathbf{E}) \mathbf{S}^T + \mathbf{V}_p, \end{aligned} \quad (6)$$

where  $\mathbf{H}^{(UR)} = [\mathbf{h}_1^{(UR)}, \dots, \mathbf{h}_K^{(UR)}] \in \mathbb{C}^{N \times K}$  is the channel from all UEs to the RIS,  $\mathbf{E} = [\mathbf{e}_1, \dots, \mathbf{e}_K] \in \mathbb{C}^{P \times K}$  is the matrix containing all coding vectors,  $\mathbf{S} = [\mathbf{s}_1, \dots, \mathbf{s}_K] \in \mathbb{C}^{T \times K}$  is the matrix containing all information symbol vectors, and  $\mathbf{V}_p \in \mathbb{C}^{M \times T}$  is the additive Gaussian noise matrix at the BS. With the properties (1) and (2), the vectorized form of  $\mathbf{Y}_p$  in the absence of noise is given by

$$\begin{aligned} \text{vec}(\mathbf{Y}_p) &= \left( \mathbf{S} \otimes \mathbf{H}^{(RB)} \right) \left( D_p(\mathbf{E}) \otimes D_p(\Phi) \right) \text{vec} \left( \mathbf{H}^{(UR)} \right) \\ &= \left( \text{vec} \left( \mathbf{H}^{(UR)} \right)^T \odot \left( \mathbf{S} \otimes \mathbf{H}^{(RB)} \right) \right) \left( \mathbf{E}_p \otimes \Phi_p \right)^T. \end{aligned} \quad (7)$$

By collecting  $\text{vec}(\mathbf{Y}_p)$  for all  $P$  time blocks, we can derive the mode-1 unfolding of the tensor  $\mathcal{Y}$  as follows:

$$\begin{aligned} [\mathcal{Y}]_1 &= [\text{vec}(\mathbf{Y}_1), \dots, \text{vec}(\mathbf{Y}_P)] \\ &= (\mathbf{S} \otimes \mathbf{H}^{(RB)}) \text{diag}(\mathbf{h}^{(UR)}) (\mathbf{E}^T \odot \Phi^T), \end{aligned} \quad (8)$$

where  $[\mathcal{Y}]_1 \in \mathbb{C}^{TM \times P}$  and  $\mathbf{h}^{(UR)} = \text{vec}(\mathbf{H}^{(UR)})$ . The channel  $\mathbf{H}^{(UR)}$  can be estimated by the vectorized form of  $[\mathcal{Y}]_1$ , i.e.,  $\mathbf{y} = \text{vec}([\mathcal{Y}]_1) = \mathbf{G}_1 \mathbf{h}^{(UR)}$ . Here we define  $\mathbf{G}_1 \in \mathbb{C}^{MPT \times NK}$  to simplify the formula, i.e.,

$$\mathbf{G}_1 = (\mathbf{E}^T \odot \Phi^T)^T \odot (\mathbf{S} \otimes \mathbf{H}^{(RB)}). \quad (9)$$

In order to estimate  $\mathbf{H}^{(RB)}$  and  $\mathbf{S}$ , we derive the mode-2 and the mode-3 unfoldings of  $\mathcal{Y}$ , i.e.,  $[\mathcal{Y}]_2 = [\mathbf{Y}_1, \dots, \mathbf{Y}_P]^T = \mathbf{G}_2 (\mathbf{H}^{(RB)})^T \in \mathbb{C}^{PT \times M}$  and  $[\mathcal{Y}]_3 = [\mathbf{Y}_1^T, \dots, \mathbf{Y}_P^T]^T = \mathbf{G}_3 \mathbf{S}^T \in \mathbb{C}^{MP \times T}$ , where

$$\mathbf{G}_2 = (\mathbf{I}_P \otimes \mathbf{S}) [\mathcal{Z}]_1 \in \mathbb{C}^{PT \times N}, \quad (10)$$

$$\mathbf{G}_3 = (\mathbf{I}_P \otimes \mathbf{H}^{(RB)}) [\mathcal{Z}]_2 \in \mathbb{C}^{MP \times K}, \quad (11)$$

where  $[\mathcal{Z}]_1 = [\mathbf{Z}_1^T, \dots, \mathbf{Z}_P^T]^T$  and  $[\mathcal{Z}]_2 = [\mathbf{Z}_1, \dots, \mathbf{Z}_P]^T$ . Here  $\mathbf{Z}_p = D_p(\Phi) \mathbf{H}^{(UR)} D_p(\mathbf{E}) \in \mathbb{C}^{N \times K}$  is introduced to simplify the expression and  $[\mathcal{Z}]_1$  and  $[\mathcal{Z}]_2$  are the mode-1 and mode-2 unfoldings of the tensor  $\mathcal{Z}$ .

### III. SEMI-BLIND JOINT CHANNEL ESTIMATION AND SYMBOL DETECTION

#### A. Stage I: Preconditioning

By utilizing the hybrid Kronecker/Khatri-Rao factorization property of the mode-1 unfolding shown in (8), we derive a closed-form (CF) solution for preconditioning containing pre-estimation and pre-detection. Assuming that the designed Khatri-Rao product matrix  $\Xi = (\mathbf{E}^T \odot \Phi^T) \in \mathbb{C}^{NK \times P}$  is full row-rank, we set  $\mathbf{Q} = [\mathcal{Y}]_1 \Xi^\dagger \in \mathbb{C}^{MT \times KN}$ . Let  $\mathbf{q}_{(k,n)}$  be the  $[(k-1)N+n]$ -th column of the matrix  $\mathbf{Q}$ , i.e.,  $\mathbf{q}_{(k,n)} = \mathbf{Q}_{\cdot, (k-1)N+n}$ ,  $n = 1, \dots, N$ , and then we obtain

$$\mathbf{q}_{(k,n)} = (\mathbf{s}_{\cdot k} \otimes \mathbf{h}_{n \cdot}^{(RB)}) h_{n,k}^{(UR)}. \quad (12)$$

Define a rank-one matrix  $\Theta_{(k,n)} = \text{unvec}(\mathbf{q}_{(k,n)}) \in \mathbb{C}^{M \times T}$  such that

$$\Theta_{(k,n)} = \mathbf{h}_{n \cdot}^{(RB)} \cdot \mathbf{s}_{\cdot k}^T \cdot h_{n,k}^{(UR)}, \quad (13)$$

where the factors  $\mathbf{h}_{n \cdot}^{(RB)}$ ,  $\mathbf{s}_{\cdot k}$  and  $h_{n,k}^{(UR)}$  can be obtained by computing the rank-one approximation of the matrix  $\Theta_{(k,n)}$  via its singular value decomposition (SVD) [5]:

$$\Theta_{(k,n)} = \mathbf{U}_{(k,n)} \Sigma_{(k,n)} (\mathbf{V}_{(k,n)})^H. \quad (14)$$

Considering the rank-one property of  $\Theta_{(k,n)}$ , we have  $\mathbf{h}_{n \cdot}^{(RB)} = \mathbf{U}_{(k,n)}(:, 1)$  for all values of  $k$ ,  $\mathbf{s}_{\cdot k} = (\mathbf{V}_{(k,n)}(:, 1))^H$  for all values of  $n$ , and  $h_{n,k}^{(UR)} = \sigma_{(k,n)}(1, 1)$  for all values of  $k$  and  $n$ . To get the pre-estimation and pre-detection of channels and symbols, respectively, we average over the  $K$  and  $N$  independent estimates of  $\mathbf{H}^{(RB)}$  and detects of  $\mathbf{S}$ . Moreover, it is assumed that the elements in the first

row of  $\mathbf{H}^{(RB)}$  and  $\mathbf{S}$  are known in order to eliminate scaling ambiguity [10]. Then, we obtain

$$\tilde{\mathbf{h}}_{n \cdot}^{(RB)} = \frac{1}{K} \sum_{k=1}^K \frac{[\mathbf{U}_{(k,n)}]_{\cdot 1}}{[\mathbf{U}_{(k,n)}]_{1,1}}, \quad (15)$$

$$\tilde{\mathbf{s}}_{\cdot k} = \frac{1}{N} \sum_{n=1}^N \frac{[\mathbf{V}_{(k,n)}]_{1 \cdot}^H}{[\mathbf{V}_{(k,n)}]_{1,1}^*}, \quad (16)$$

$$\tilde{h}_{n,k}^{(UR)} = [\mathbf{U}_{(k,n)}]_{1,1} [\Sigma_{(k,n)}]_{1,1} [\mathbf{V}_{(k,n)}]_{1,1}. \quad (17)$$

By exploiting the preconditioning operation, we acquire the initial values of  $\mathbf{H}^{(UR)}$ ,  $\mathbf{H}^{(RB)}$  and  $\mathbf{S}$ .

#### B. Stage II: Iterative Fitting

Stage II begins with the initialization from stage I. From the vectorized form of  $[\mathcal{Y}]_1$ , i.e.,  $\mathbf{y}$ , we use the LS fitting to obtain the estimated vectorized form of  $\mathbf{H}^{(UR)}$  as

$$\hat{\mathbf{h}}^{(UR)} = \arg \min_{\mathbf{h}^{(UR)}} \left\| \mathbf{y} - \hat{\mathbf{G}}_1 \mathbf{h}^{(UR)} \right\|_2^2 = (\hat{\mathbf{G}}_1)^\dagger \mathbf{y}. \quad (18)$$

Next, from the mode-2 unfolding of tensor  $\mathcal{Y}$ , we exploit the LS fitting to obtain the estimated  $\mathbf{H}^{(RB)}$  with the vector  $\hat{\mathbf{h}}^{(UR)}$  as

$$\hat{\mathbf{H}}^{(RB)} = \arg \min_{\mathbf{H}^{(RB)}} \left\| [\mathcal{Y}]_2 - \hat{\mathbf{G}}_2 (\mathbf{H}^{(RB)})^T \right\|_F^2 = \left( (\hat{\mathbf{G}}_2)^\dagger [\mathcal{Y}]_2 \right)^T. \quad (19)$$

Supposing that the number of resolvable paths (NRPs) between each channel is known, the estimation of  $\mathbf{H}^{(RB)}$  can be optimized at every iteration via the singular value projection (SVP) method by utilizing the low-rank structure of the mmWave channel [11], i.e.,

$$\left( \hat{\mathbf{H}}^{(RB)} \right)_{\text{opt}} = \text{SVP} \left( \hat{\mathbf{H}}^{(RB)} \right) = \sum_{l_{RB}=1}^{L_{RB}} \mathbf{u}_{l_{RB}} \varepsilon_{l_{RB}} \mathbf{v}_{l_{RB}}^T, \quad (20)$$

where  $\varepsilon$  represents the maximum significant singular value, while  $\mathbf{u}$  and  $\mathbf{v}$  correspond to the left and right singular vectors, respectively. Then, from the mode-3 unfolding of tensor  $\mathcal{Y}$ , we utilize the LS fitting to update  $\mathbf{S}$  with the vector  $\hat{\mathbf{h}}^{(UR)}$  and the optimized matrix  $\left( \hat{\mathbf{H}}^{(RB)} \right)_{\text{opt}}$ , i.e.,

$$\hat{\mathbf{S}} = \arg \min_{\mathbf{S}} \left\| [\mathcal{Y}]_3 - \hat{\mathbf{G}}_3 \mathbf{S}^T \right\|_F^2 = \left( (\hat{\mathbf{G}}_3)^\dagger [\mathcal{Y}]_3 \right)^T. \quad (21)$$

The error of the  $i$ -th iteration can be calculated as

$$\xi(i) = \left\| \mathbf{y} - \hat{\mathbf{G}}_1(i) \mathbf{h}^{(UR)}(i) \right\|_2^2 / \left\| \mathbf{y} \right\|_2^2, \quad (22)$$

and the convergence is decided when  $\xi(i) - \xi(i-1) \leq \delta$ , where  $\delta$  is the error tolerance. The proposed two-stage algorithm is summarized in Table I.

### IV. IDENTIFIABILITY AND UNIQUENESS

For system identifiability, sufficient and necessary conditions are satisfied when the parameters of the pseudo-inverse operators obtained by minimizing the LS cost functions are full row-rank or full column-rank. In the first stage, an accurate

TABLE I  
The Two-Stage Fitting Algorithm

**Input:** Received tensor  $\mathcal{Y}$ , RIS phase shift matrix  $\Phi$  and encoding matrix  $\mathbf{E}$ .

—————*Start Stage I*—————

- 1.1 For  $n = 1, \dots, N$  and  $k = 1, \dots, K$ 
  - (a) Calculate  $\mathbf{Q} = [\mathcal{Y}]_1 \Xi^\dagger$ ;
  - (b) Reshape  $\mathbf{q}_{(k,n)}$  as the matrix  $\Theta_{(k,n)}$ ;
  - (c) Calculate the SVD of  $\Theta_{(k,n)}$ ;
  - (d) Eliminate scaling ambiguity;
  - (e) Output the initializations of  $\mathbf{H}^{(UR)}$ ,  $\mathbf{H}^{(RB)}$  and  $\mathbf{S}$ ;

1.2 End for

—————*Start Stage II*—————

- 2.1 Initialize  $\hat{\mathbf{S}}(0)$  and  $\hat{\mathbf{H}}^{(RB)}(0)$  from 1.1(e);
- 2.2 Set  $i = 0$ ;
- 2.3  $i \leftarrow i + 1$ ;
- 2.4 Calculate the LS estimate of  $\hat{\mathbf{h}}^{(UR)}(i)$  by (18);
- 2.5 Calculate the LS estimate of  $\hat{\mathbf{H}}^{(RB)}(i)$  by (19);
- 2.6 Apply SVP method to  $\hat{\mathbf{H}}^{(RB)}(i)$  by (20);
- 2.7 Calculate the LS estimate of  $\hat{\mathbf{S}}(i)$  by (21);
- 2.8 Calculate  $\xi(i)$  by (22);
- 2.9 Repeat steps 2.3 to 2.9 until convergence;
- 2.10 Eliminate scaling ambiguity.

**Output:** The estimated matrices  $\mathbf{H}^{(UR)}$ ,  $\mathbf{H}^{(RB)}$  and  $\mathbf{S}$ .

initialization is completed when the designed matrix  $\Xi$  is full row-rank. However, even if this assumption is not satisfied, we can still obtain partial information of channels and symbols. On this foundation, the preconditioning operation accelerates computing and makes the subsequent iterative fitting algorithm more stable. In the second stage, from the LS solutions (18), (19) and (21), the identifiability of the triple  $(\mathbf{H}^{(UR)}, \mathbf{H}^{(RB)}, \mathbf{S})$  requires that  $\mathbf{G}_1$ ,  $\mathbf{G}_2$  and  $\mathbf{G}_3$  are full column-rank.

On the premise of meeting identifiability conditions, the triple  $(\hat{\mathbf{H}}^{(UR)}, \hat{\mathbf{H}}^{(RB)}, \hat{\mathbf{S}})$  obtained by the PARATUCK2 decomposition is not completely equal to the original  $(\mathbf{H}^{(UR)}, \mathbf{H}^{(RB)}, \mathbf{S})$ , i.e., the PARATUCK2 decomposition is essentially unique and there exists permutation and column scaling ambiguities [10]. Supposing that the matrices  $\Phi$  and  $\mathbf{E}$  as well as the first row of  $\mathbf{S}$  and  $\mathbf{H}^{(RB)}$  are known at the BS, we have

$$\mathbf{S} = \hat{\mathbf{S}} \Delta^{(S)}, \quad (23)$$

$$\mathbf{H}^{(RB)} = \hat{\mathbf{H}}^{(RB)} \Delta^{(RB)}, \quad (24)$$

$$\mathbf{H}^{(UR)} = \Delta^{(RB)-1} \hat{\mathbf{H}}^{(UR)} \Delta^{(S)-1}, \quad (25)$$

where  $\Delta^{(S)} = D_1(\mathbf{S})D_1^{-1}(\hat{\mathbf{S}})$  and  $\Delta^{(RB)} = D_1(\mathbf{H}^{(RB)})D_1^{-1}(\hat{\mathbf{H}}^{(RB)})$ . Thus, the proposed semi-blind algorithm can eliminate the inherent ambiguity with few pilot sequences. In practice, we can consider integrating the sensing devices into the RIS to estimate the first row of  $\mathbf{H}^{(RB)}$  or the first column of  $\mathbf{H}^{(UR)}$  [12]. Meanwhile, we

consider embedding the information known to the BS into the first row of  $\mathbf{S}$ .

## V. RESULTS AND DISCUSSIONS

In this section, numerical results are reported to assess the performance of the proposed algorithm on the normalized mean square error (NMSE) and the bit error rate (BER). The default values of the adopted system parameters are as follows:  $K = 2$ ,  $N = 36$  ( $N_1 = N_2 = 6$ ),  $M = 16$  ( $M_1 = M_2 = 4$ ),  $T = 8$ ,  $P = 60$ ,  $L_{UR} = L_{UR,k} = 2$  for all  $k = 1, \dots, K$ , and  $L_{RB} = 2$ . 16QAM is considered to modulate the information symbols. All simulation results are acquired by averaging over 10000 Monte Carlo runs.  $|\alpha_l^k| = 10^{-2}d_{UR,k}^{-2.6}$  and  $|\beta_l| = 10^{-2}d_{RB}^{-2.2}$ , where  $d_{UR,k}$  is the distance from the  $k$ -th UE to the RIS and is equal to  $100m$  for all  $k = 1, \dots, K$ , while  $d_{RB}$  is the distance from the RIS to the BS and is equal to  $10m$  [13]. The elements in the RIS phase shift matrix  $\Phi$  are chosen from  $\{-1/\sqrt{P}, +1/\sqrt{P}\}$  by utilizing discrete phase shifts (DFT) of the RIS. The coding matrix  $\mathbf{E}$  is generated such that  $e_{p,k} = \exp(-j2\pi c)/\sqrt{P}$ , where  $c$  is a random variable chosen from the standard uniform distribution.

In the first example, we compare the performance of the proposed algorithm with the pilot-assisted BALS algorithm [5], the semi-blind KAKF algorithm [7], and the pilot-assisted CF algorithm [14]. Moreover, we also plot the curve of the proposed algorithm without NRPs. A fair comparison with the pilot-assisted methods is assumed. For the pilot-assisted algorithms, the same time block of information symbols and pilots is repeated  $P'$  times, which means that the coherence time of the pilot-assisted algorithms is  $T_{CP} = (T' + T_p)P'$ , where  $T'$  is the length of the symbol and  $T_p$  is the length of the pilot. In this example, we assume  $P' = 60$ ,  $T' = 6$ , and  $T_p = 2$ , which implies the time to transmit useful information for different algorithms is the same. From the channel NMSE and symbol BER curves depicted in Figs. 2 and 3, respectively, we observe that the proposed algorithm outperforms the competitive algorithms whether in channel estimation or symbol detection. The result originates from the fact that the proposed algorithm is optimized by preconditioning and further improves performance with iterative fitting. On the other hand, by means of the low-rank structure of the mmWave channel, the algorithm with NRPs meliorates the channel estimation and symbol detection performance. In addition, since the designed matrix is not full row-rank, the semi-blind KAKF algorithm cannot effectively estimate channels and detect symbols. However, the final accuracy of the proposed algorithm is almost unchanged when the designed matrix is not full row-rank. In this case, the performance of the preconditioning will be affected, thereby only affecting the fitting speed of the algorithm.

The dominant complexity of the pilot-assisted BALS algorithm, the semi-blind KAKF algorithm, the pilot-assisted CF algorithm, and the proposed algorithm with or without NRPs can be estimated by  $\mathcal{O}((KN + MN + MK)PN)$ ,  $\mathcal{O}(MNTK \min\{MN, TK\})$ ,  $\mathcal{O}(KMN(P + \min\{K, M\}))$  and  $\mathcal{O}(PMTK^2N^2)$ , respectively. Although the competitive algorithms have lower complexity, their estimation and detec-

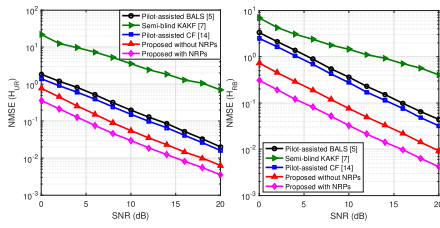


Fig. 2. NMSE versus SNR compared with different algorithms.

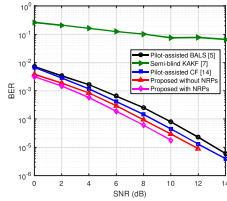


Fig. 3. BER versus SNR compared with different algorithms.

tion accuracy is inferior to that of the proposed algorithm. In addition, the number of the iterations is reduced to about 4 at high SNR with the preconditioning for the proposed algorithm, which implies that the complexity gap with the competitive algorithms is reduced.

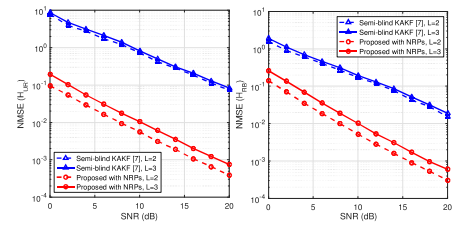
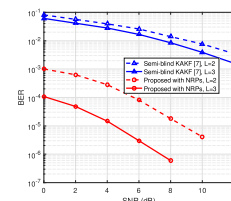
In the second example, we analyze the NMSE and BER performance of the proposed algorithm and the semi-blind KAKF algorithm for different numbers of  $L_{UR}$  and  $L_{RB}$ , where  $K = 4$ ,  $P = 160$ , and we set  $L = L_{RB} = L_{UR} = L_{UR,k}$  for all  $k = 1, \dots, K$ . For the proposed algorithm, since the low-rank structure of the mmWave channel matrix is utilized, the NMSE performance of  $\mathbf{H}^{(UR)}$  and  $\mathbf{H}^{(RB)}$  deteriorates with the increase of  $L$  as shown in Fig. 4. From Fig. 5, we observe that the BER performance improves with the increase of  $L$ . The reason for this result is that the spatial diversity gain improves with the raise of  $L$ . Moreover, we see from Figs. 4 and 5 that the NMSE and BER performance of the proposed algorithm is significantly better than that of the semi-blind KAKF algorithm, even when the designed matrix is full row-rank.

## VI. CONCLUSION

In this letter, we developed a semi-blind joint channel estimation and symbol detection scheme for RIS-empowered multiuser mmWave systems. By applying the decomposition property of the constructed PARATUCK2 tensor model, we acquired full knowledge of CSI involved in the communication and information symbols of all UEs without a dedicated training stage. Simulation results show that the proposed scheme yields smaller channel estimation and symbol detection error compared with the existing methods. In the future, we will further extract channel parameters such as directions of arrival/departure (DoAs/DoDs), time delays and complex path gains for the user localization by extending the PARATUCK2 decomposition to higher-order tensors.

## REFERENCES

[1] Y. Liu, S. Zhang, F. Gao, J. Tang, and O. A. Dobre, "Cascaded channel estimation for RIS assisted mmwave MIMO transmissions," *IEEE Wireless Commun. Lett.*, vol. 10, no. 9, pp. 2065–2069, Jun. 2021.

Fig. 4. NMSE versus SNR for different  $L$ .Fig. 5. BER versus SNR for different  $L$ .

- [2] Z. Wang, L. Liu, and S. Cui, "Channel estimation for intelligent reflecting surface assisted multiuser communications: Framework, algorithms, and analysis," *IEEE Trans. Wireless Commun.*, vol. 19, no. 10, pp. 6607–6620, Oct. 2020.
- [3] X. Guan, Q. Wu, and R. Zhang, "Anchor-assisted channel estimation for intelligent reflecting surface aided multiuser communication," *IEEE Trans. Wireless Commun.*, vol. 21, no. 6, pp. 3764–3778, Jun. 2022.
- [4] L. Wei, C. Huang, G. C. Alexandropoulos, C. Yuen, Z. Zhang, and M. Debbah, "Channel estimation for RIS-empowered multi-user MISO wireless communications," *IEEE Trans. Commun.*, vol. 69, no. 6, pp. 4144–4157, Mar. 2021.
- [5] G. T. de Araújo, A. L. F. de Almeida, and R. Boyer, "Channel estimation for intelligent reflecting surface assisted MIMO systems: A tensor modeling approach," *IEEE J. Sel. Top. Signal Process.*, vol. 15, no. 3, pp. 789–802, Feb. 2021.
- [6] L. Wei, C. Huang, Q. Guo, Z. Yang, Z. Zhang, G. C. Alexandropoulos, M. Debbah, and C. Yuen, "Joint channel estimation and signal recovery for RIS-empowered multiuser communications," *IEEE Trans. Commun.*, vol. 70, no. 7, pp. 4640–4655, Jul. 2022.
- [7] G. T. de Araújo, P. R. B. Gomes, A. L. F. de Almeida, G. Fodor, and B. Makki, "Semi-blind joint channel and symbol estimation in IRS-assisted multiuser MIMO networks," *IEEE Wireless Commun. Lett.*, vol. 11, no. 7, pp. 1553–1557, Jul. 2022.
- [8] R. W. Heath, N. González-Prelcic, S. Rangan, W. Roh, and A. M. Sayeed, "An overview of signal processing techniques for millimeter wave MIMO systems," *IEEE J. Sel. Top. Signal Process.*, vol. 10, no. 3, pp. 436–453, Feb. 2016.
- [9] C. Hu, L. Dai, T. Mir, Z. Gao, and J. Fang, "Super-resolution channel estimation for mmwave massive MIMO with hybrid precoding," *IEEE Trans. Veh. Technol.*, vol. 67, no. 9, pp. 8954–8958, Jun. 2018.
- [10] R. A. Harshman and M. E. Lundy, "Uniqueness proof for a family of models sharing features of tucker's three-mode factor analysis and parafac/candecomp," *Psychometrika*, vol. 61, no. 1, pp. 133–154, Mar. 1996.
- [11] J. Du, M. Han, Y. Chen, L. Jin, and F. Gao, "Tensor-based joint channel estimation and symbol detection for time-varying mmwave massive MIMO systems," *IEEE Trans. Signal Process.*, vol. 69, pp. 6251–6266, Nov. 2021.
- [12] Q. Wu, S. Zhang, B. Zheng, C. You, and R. Zhang, "Intelligent reflecting surface-aided wireless communications: A tutorial," *IEEE Trans. Commun.*, vol. 69, no. 5, pp. 3313–3351, May 2021.
- [13] Q. Wu and R. Zhang, "Beamforming optimization for wireless network aided by intelligent reflecting surface with discrete phase shifts," *IEEE Trans. Commun.*, vol. 68, no. 3, pp. 1838–1851, Dec. 2020.
- [14] K. Ardah, S. Ghorekhloo, A. L. F. de Almeida, and M. Haardt, "Trice: A channel estimation framework for RIS-aided millimeter-wave MIMO systems," *IEEE Signal Process. Lett.*, vol. 28, pp. 513–517, Feb. 2021.